Mem. S.A.It. Vol. 88, 530

Memorie della

Properties, rotation of molecular clouds in M 33

J. Braine

Laboratoire d'Astrophysique de Bordeaux, Univ. Bordeaux, CNRS, B18N, allée Geoffroy Saint-Hilaire, 33615 Pessac, France, e-mail: `jonathan.braine@u-bordeaux.fr`

Abstract. The sample of 566 molecular clouds (Corbelli et al. 2017) identified in the CO(2–1) IRAM survey (Druard et al. 2014) covering the disk of M 33 is explored in detail.

Key words. Galaxies: Individual: M 33 – Galaxies: ISM – ISM: clouds – Stars: Formation

1. Introduction

The clouds were found using CPROPS (Rosolowsky & Leroy 2006) and were subsequently catalogued in terms of their star-forming properties as non-star-forming (A), with embedded star formation (B), or with exposed star formation (C, e.g. presence of Hα emission) – see Gratier et al. (2012) and Corbelli et al. (2017) for details. Starting with this base, we find that the size-linewidth relation among the M 33 clouds is quite weak but, when comparing with clouds in other nearby galaxies, the linewidth decreases for any given cloud size, with metallicity (see Fig. 2). The linewidth and particularly the line brightness decrease with galactocentric distance. The large number of clouds makes it possible to calculate well-sampled cloud mass spectra and mass spectra of subsamples. As noted earlier, but considerably better defined here, the mass spectrum steepens (i.e. higher fraction of small clouds) with galactocentric distance. A new finding is that the mass spectrum of A clouds is much steeper than that of the star-forming clouds. Further dividing the sample, this difference is strong at both large and small galactocentric distances and the A vs C difference is a stronger effect than the inner/outer difference in mass spectra (Fig. 3). Velocity gradients are identified in the clouds using standard techniques in which the first moment (intensity weighted velocity) of each position within the cloud is calculated and a plane (i.e. linear velocity gradient) is fit. The coefficients of the plane are equivalent to a velocity gradient. The gradients are weak and are dominated by prograde rotation; the effect is stronger for the high signal-to-noise clouds (see Fig. 4). The S/N of this dataset is much higher than in previous work and presumably this is why cloud rotation was not clearly detected previously (Rosolowsky et al. 2003; Imara et al. 2011). The angular momenta are low but compatible with at least some simulations (see Fig. 5). Finally, the cloud velocity gradients are compared with overall galactic rotation, calculated in the same way. The cloud and galactic gradients are similar; the cloud rotation periods are much longer than cloud lifetimes and comparable to the galactic rotation period. The rotational kinetic energy is $1-2\%$ of the gravitational potential energy and the cloud edge velocity is well below the escape velocity, such that cloud-scale rotation probably has little influence of the evolution of molecular clouds. This argues against

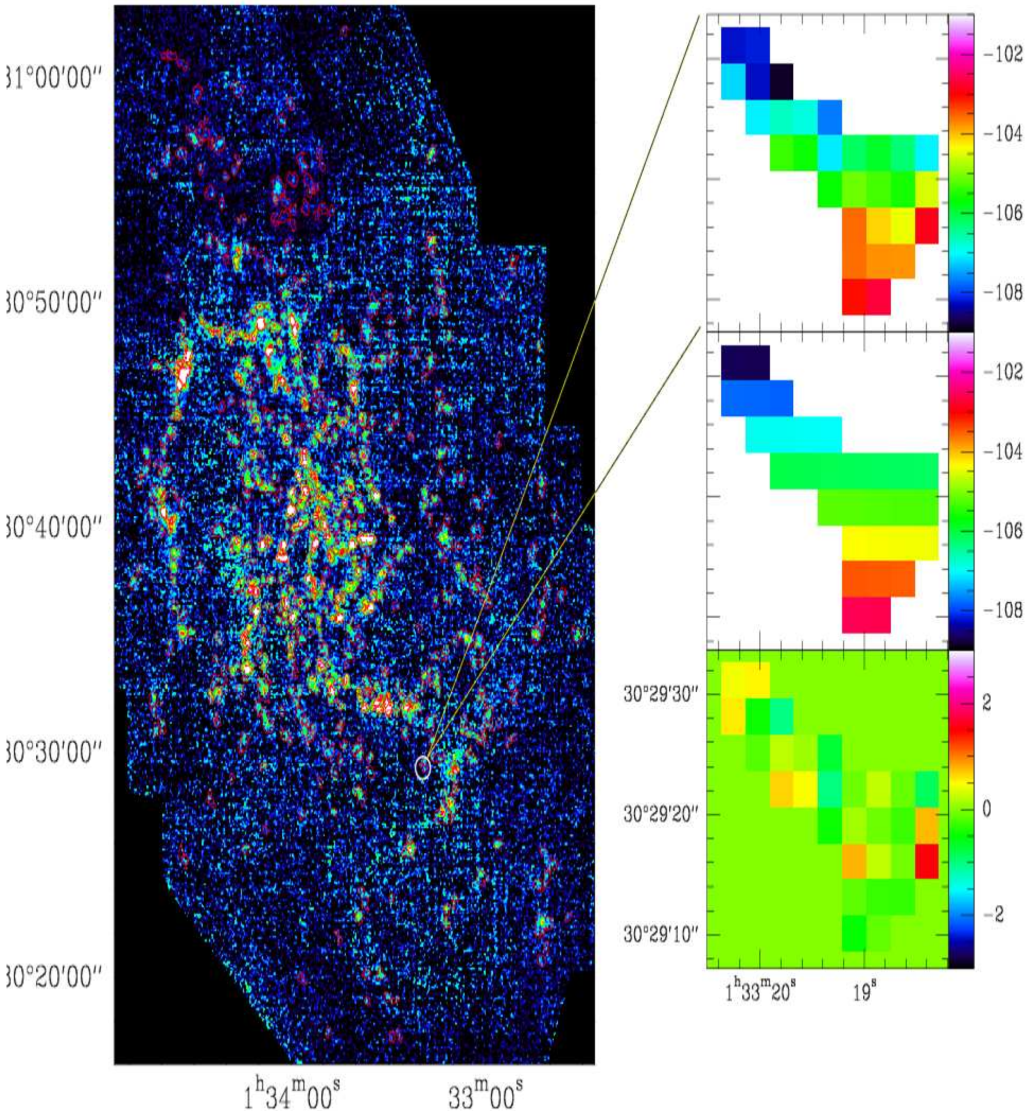

Fig. 1. (left) CO(2–1) integrated intensity map of M33 with the cloud contours superposed in red and a zoom on cloud #4 showing (top right) the velocities $v_{(x,y)}$ as explained below, (middle right) the fit to the velocities, and to the bottom right the velocity residual ($v - v_{\rm fit}$). This cloud (#4 in the catalog) was chosen to illustrate the process for its rather clear gradient despite its elongated form. The first moment is calculated as follows: $v_{(x,y)} = \sum_{i=cen-2}^{i=cen+2} v_i T_i dv / \sum_{i=cen-2}^{i=cen+2} T_i dv$. The plane is fit as $v_{(x,y)} = ax + by + c$, where $a = \frac{\partial v}{\partial x} = \frac{\partial v}{\partial RA}$ and $b = \frac{\partial v}{\partial y} = \frac{\partial v}{\partial Dec}$ because x and y are the pixel numbers following the RA and Dec directions. It is worth noting that there is emission which CPROPS was not able to decompose into clouds and that the fraction of the CO emission not decomposed into clouds increases with radius.

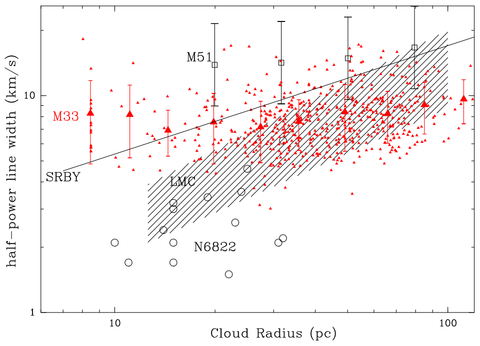

Fig. 2. Size-linewidth relation for M33 clouds (red) and other galaxies observed with similar or better angular resolution. Large red symbols are the binned M33 data with error bars indicating dispersion. The non-M 33 clouds are shown as black symbols. The region populated by LMC clouds is hatched and the M51 data (squares) are binned averages. The line labelled SRBY is the Solomon et al. (1987) relation for the Galaxy.

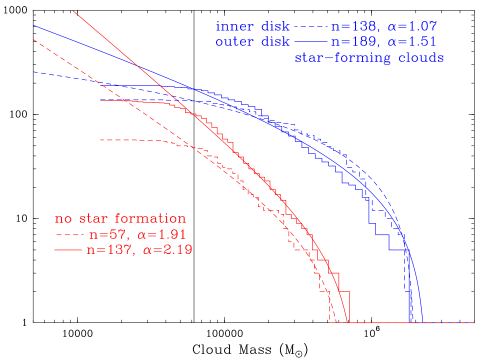

Fig. 3. Similar to Fig. 2 of Gratier et al. (2012) but separating inner and outer disk A and C clouds. It is immediately apparent that galactocentric distance is less important than star formation. The number of clouds and the slope of the mass function are given for each group. See text for further details.

strong cloud-cloud interactions as simulations show they tend to increase angular momenta.

References

Corbelli, E., et al. 2017, A&A, 601, A146
Dobbs, C. L. 2008, MNRAS, 391, 844
Druard, C., et al. 2014, A&A, 567, A118
Gratier, P., et al. 2012, A&A, 542, 108

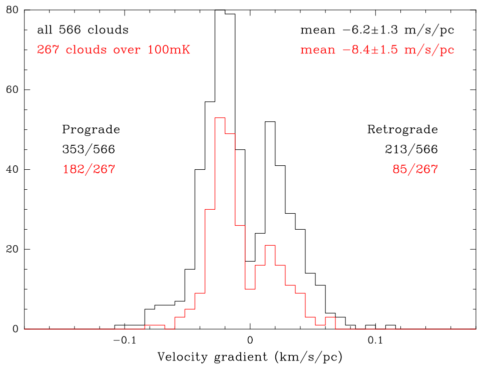

Fig. 4. Cloud velocity gradients – for the entire sample in black and for only the stronger clouds in red, where the line temperature averaged over the whole cloud is over 100mK T_a^*. Prograde rotation is given a negative sign here because the galaxy rotation velocity increases with decreasing declination.

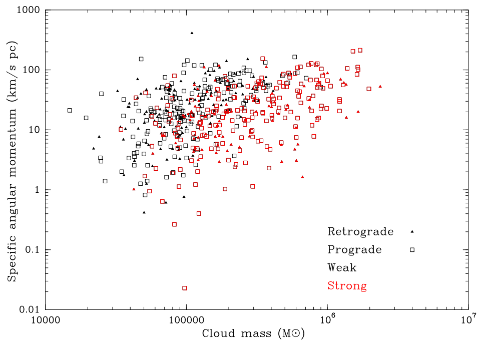

Fig. 5. Specific angular momenta of the M33 clouds. Red lines or symbols indicate data for the CO-strong clouds. The asymmetry favoring prograde gradients (Fig. 4) is also present for the angular momenta. The variation of angular momentum with cloud mass is very weak; this figure can be directly compared with Fig. 8 of the Dobbs (2008) simulations. The values in this figure include a factor 1.6 in angular velocity to account for the beam-smearing due to the (relatively) large beamsize.

Imara, N., Bigiel, F., & Blitz, L. 2011, ApJ, 732, 79
Rosolowsky, E., et al. 2003, ApJ, 599, 258
Rosolowsky, E. & Leroy, A. 2006, PASP, 118, 590
Solomon, P. M., et al. 1987, ApJ, 319, 730